Molecular Therapy
Nucleic Acids
Original Article

# MSCs act as biopatches for blood-retinal barrier preservation to enhance functional recovery after retinal I/R

Xiaoyue Wei,[1,4] Hanyiqi Mu,[2,4] Qinmu Zhang,[2,4] Ziyuan Zhang,[2] Yifei Ru,[2] Kunbei Lai,[1] Yuan Ma,[1] Zhuangling Lin,[1] Rebiya Tuxun,[1] Zitong Chen,[1] Andy Peng Xiang,[3] and Tao Li[1]

[1]State Key Laboratory of Ophthalmology, Zhongshan Ophthalmic Center, Sun Yat-Sen University, Guangzhou 510230, China; [2]Zhongshan School of Medicine, Sun Yat-Sen University, Guangzhou 510080, China; [3]Center for Stem Cell Biology and Tissue Engineering, Key Laboratory for Stem Cells and Tissue Engineering, Ministry of Education, Sun Yat-Sen University, Guangzhou 510080, China

**Retinal ischemia/reperfusion (I/R) is one of the most common pathologies of many vision-threatening diseases and is caused by blood-retinal barrier (BRB) breakdown and the resulting inflammatory infiltration. Targeting BRB is promising for retinal I/R treatment. Mesenchymal stromal cells (MSCs) are emerging as novel therapeutic strategies. Although intravitreal injection targets the retina, the restricted number of injected cells still requires the precise biodistribution of MSCs near the injury site. Here, we found that retinal I/R led to BRB breakdown, which induced protein and cell leakage from the circulation. Retinal cell death and diminished visual function were subsequently detected. Moreover, the expression of the chemokine CCL5 increased after retinal I/R, and CCL5 colocalized with the BRB. We then overexpressed CCR5 in human induced pluripotent stem cell-derived MSCs (iMSCs). *In vivo*, intravitreal-injected iMSC$^{CCR5}$ preferentially migrated and directly integrated into the BRB, which preferably restored BRB integrity and eventually promoted retinal function recovery after retinal I/R. In summary, our work suggested that iMSCs act as biopatches for BRB preservation and that iMSC-based therapy is a promising therapeutic approach for retinal diseases related to I/R.**

## INTRODUCTION

Retinal ischemia/reperfusion (I/R), a process whereby initial ischemia and subsequent recovery of the blood supply in the retina occur,[1] is one of the most common pathological processes in many vision-threatening diseases, including glaucoma, diabetic retinopathy, and central retinal artery occlusion,[2,3] and causes 4.68 million cases of blindness per year worldwide.[4] Current clinical interventions, including pars plana vitrectomy and anti-vascular endothelial growth factor (VEGF) injection, target only the middle-to-late stages of retinal I/R-related diseases, such as vitreous hemorrhage or neovascularization, when vision loss is likely irreversible.[5] Pathologically, unlike in peripheral organs, retinal I/R first leads to the disruption of specialized vascular barrier integrity and the blood-retinal barrier (BRB) and then results in inflammatory infiltration, ultimately causing a self-reinforcing destructive cascade involving ganglion cell apoptosis and microglial activation.[6,7] Hence, an effective way to restore BRB integrity and eventually terminate this microenvironmental cascade at the early stage is promising for clinical transition.

Mesenchymal stromal cells (MSCs) represent a promising cell-based therapeutic option for refractory ocular diseases.[8,9] On the one hand, MSC extracts, including extracellular vesicles (EVs) and microRNAs, alleviate retinal injuries through various biochemical mechanisms.[10,11] The administration of MSC-derived EVs (MSC-EVs) in a glaucoma model enhances retinal function recovery by decreasing neuroinflammation and apoptosis in retinal tissue.[11] MicroRNA192 from MSC-EVs relieves the inflammatory response and angiogenesis in oxygen-induced retinopathy.[10] On the other hand, MSCs provide structural support for specialized structures that MSC extracts do not preform. MSCs improve fracture healing by directly targeting the injury site and functioning as bioscaffolds for osteogenesis.[12,13] Additionally, for barrier preservation, MSCs contribute to the vasoconstriction capacity of the blood-brain barrier (BBB), mimicking an *in vitro* model.[14] Thus, we speculated that MSCs could patch the BRB by providing structural support in retinal I/R *in vivo*. However, primary MSCs have limited passages *in vitro* and exhibit biological and functional heterogeneity, which may raise concerns about their safety and effectiveness.[15] Previous study in our lab has generated highly homogeneous MSCs derived from human induced pluripotent stem cells (hiPSCs), which showed considerable similarity in function.[16] Moreover, since hiPSCs can differentiate into homogeneous MSCs in a large quantity,[17] hiPSC-derived MSCs (iMSCs) can be a homogeneous and unlimited source for cell therapy in future clinical

Received 18 June 2024; accepted 30 December 2024;
https://doi.org/10.1016/j.omtn.2024.102445.

[4]These authors contributed equally

**Correspondence:** Andy Peng Xiang, Center for Stem Cell Biology and Tissue Engineering, Sun Yat-Sen University, Guangzhou, Guangdong, China.
**E-mail:** xiangp@mail.sysu.edu.cn
**Correspondence:** Tao Li, State Key Laboratory of Ophthalmology, Zhongshan Ophthalmic Center, Sun Yat-Sen University, Guangzhou, Guangdong, China.
**E-mail:** litao2@mail.sysu.edu.cn

applications.[18] Other obstacles limiting the clinical application of MSCs include their unsatisfactory homing and planting capacity.[19,20] For retinal disease treatment, although intravitreal injection targets the retina, the restricted number of injected cells still requires the precise biodistribution of MSCs near the injury site.[21,22]

Chemokine ligands and chemokine receptors guide the directional trafficking of MSCs not only for organ-specific migration but also for niche-specific distribution within organs. MSCs can help repair diabetic skin wounds, where they transdifferentiate into multiple skin cell types to assist regenerative wound healing via the CXCL16-CXCR6 axis.[23] Additionally, the CXCL12-CCR4 axis plays an important role in the homing of MSCs to the hematopoiesis niche in the bone marrow,[24,25] while the CCL3-CCR1 axis is involved in MSC migration to bone fracture sites for osteogenesis.[26] Therefore, we hypothesized that genetically edited iMSCs that express the proper chemokine receptor would migrate to the BRB, improve BRB integrity, and eventually promote retinal function recovery after retinal I/R.

## RESULTS

### BRB disruption after retinal I/R

To investigate the impact of I/R on retinal tissue, we first established a retinal I/R model through internal carotid artery (ICA) occlusion (ICAO) (Figure S1A) and employed immunofluorescence staining to assess the integrity of the BRB at 6 h, 1 day, and 3 days after retinal I/R, which can be reflected by tight junction coverage and pericyte coverage.[27,28] The integrity of Claudin5, a tight junction protein, and pericyte coverage were compromised after retinal I/R and deteriorated over time (Figures 1A–1D). The integrity of ZO-1, another tight junction protein of the BRB, also decreased at 1 day after retinal I/R (Figures S1B and S1D). For further verification, we focused on the leakage of serum protein and red blood cells (RBCs) in retinal tissue. Immunofluorescence staining revealed serum protein fibrinogen leakage and RBC leakage into retinal tissue after retinal I/R, which increased over time (Figures 1E–1H). Additionally, F4/80$^{+}$ macrophages emigrated from blood vessels and infiltrated retinal tissue after retinal I/R (Figures S1C and S1E). Taken together, these results confirmed that retinal I/R resulted in the breakdown of the BRB, which deteriorated over time. Since the resulting inflammatory infiltration is an essential driver of the destructive retinal I/R cascade,[29] retinal cell death was determined via *in situ* terminal deoxynucleotidyl transferase dUTP nick-end labeling (TUNEL) staining. For completeness of inquiry and clarity of expression, we artificially divided the retina into three different positions according to the anatomy, including the center (within 200 μm of the optic disc), far-periphery (retinal margin), and mid-periphery (between the 2 positions stipulated above). Retinal section staining revealed that the degree of apoptosis at each position increased with time after retinal I/R (Figures 1I and 1J).

### The expression of CCL5 increased after retinal I/R

There are multiple mechanisms underlying I/R injury, including calcium overload, oxidative stress, and mitochondrial dysfunction.[30,31] Retinas from the sham and I/R groups were obtained 1 day after retinal I/R for transcriptome sequencing to investigate changes in the retinal microenvironment and outstanding pathways after retinal I/R and identify potential therapeutic targets. Kyoto Encyclopedia of Genes and Genomes (KEGG) analysis suggested that the interaction of chemokines and corresponding receptors might play an important role (Figure 2A), and the spectrum of chemokines changed greatly after retinal I/R (Figure S2A). Considering that the chemokine/chemokine receptor axis is indispensable for MSC migration, we next obtained retinas 1 day after retinal I/R to detect the mRNA levels of chemokines, which were reported to be associated with I/R changes,[32,33] including CCL2, CCL5, CCL7, CCL12, CXCL2, and CXCL12, and found that the mRNA level of *Ccl5* increased most markedly (Figure 2B). Furthermore, the mRNA level of *Ccl5* peaked at 1 day after retinal I/R (Figure 2C), suggesting the potential optimal therapeutic timing. Moreover, flow cytometry analysis revealed that the expression of CCL5 in retinas increased at 1 day after retinal I/R (Figures 2D and 2E). Since retinal I/R leads to BRB damage, we next explored the relationship between CCL5 and the BRB. Immunofluorescence staining revealed that more than 50% of the vessels colocalized with CCL5 in the superficial, intermediate, and deep layers (Figures 2F, 2G, and S3A), which suggested that retinal vessels could be targeted via the CCL5-CCR5 axis. In addition, gene set enrichment analysis (GSEA) revealed microenvironmental changes, including immune activation, matrix and vasculature reorganization and neuronal system degeneration in the retina after retinal I/R (Figures S4A–S4C). Together, these results presented that the expression of CCL5 increased and peaked at 1 day after retinal I/R in the retina and that CCL5 prominently colocalized with the BRB, suggesting that targeting the BRB via chemotaxis of CCL5 at 1 day after retinal I/R could be promising.

### Overexpression of CCR5 improved the migratory capacity of iMSCs in response to CCL5

MSC-based therapy may serve as a potential intervention for retinal I/R-related diseases. To eliminate the heterogeneity of MSCs, we differentiated hiPSCs, which expressed stemness markers, including Nanog, Oct4, and Sox2 (Figure S5B), into MSCs according to methods reported previously (Figure S5A).[16] iMSCs still had adipogenic, osteogenic, and chondrogenic potential (Figure S5C) and exhibited a typical MSC surface pattern in which CD29, CD44, CD73, and CD90 were positive and CD34 and CD45 were negative (Figure S5D). Next, in light of increased CCL5 colocalization with the BRB after retinal I/R, we speculated that iMSCs could be recruited to the damaged BRB via the CCL5-CCR5 axis, which may improve the effect of MSC-based therapy. Considering that MSCs express chemokine receptors at an almost negligible level,[34] we transduced iMSCs with lentiviral vectors encoding CCR5 (referred to as iMSC$^{CCR5}$) or tdTomato (referred to as iMSC$^{tdTomato}$) to increase CCR5 expression. The cells expressing tdTomato fluorescence were isolated via flow cytometry, and the mRNA and protein levels of CCR5 were determined (Figures S5E–S5G).

We next focused on the migratory capacity of iMSC$^{CCR5}$ in response to CCL5. First, we compared the migratory capacity of iMSC$^{CCR5}$ and

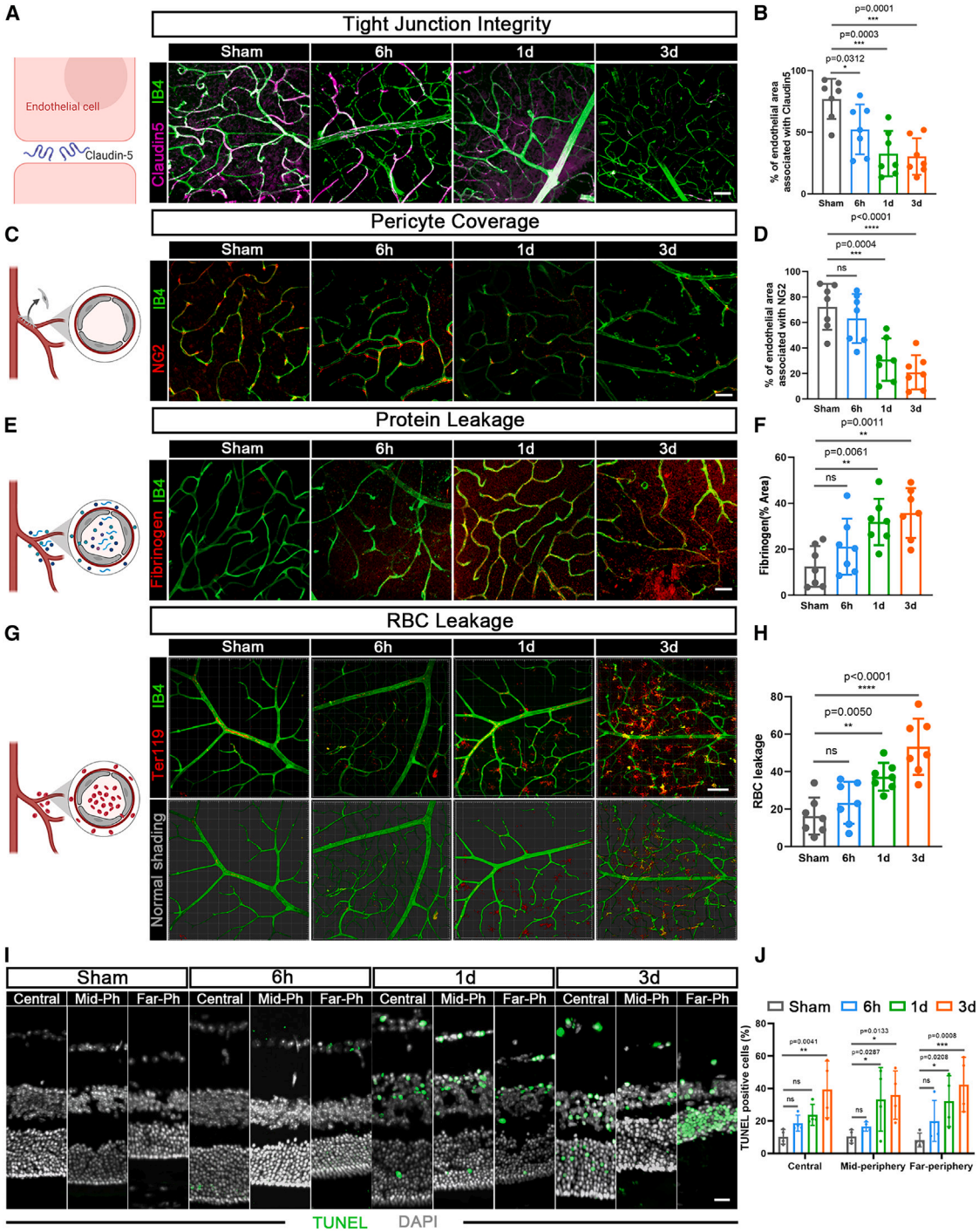


**Figure 1. BRB breakdown after retinal I/R**

(A, C, E, and G) Patterns (left) and representative confocal fluorescence images (right) of the distribution of Claudin5 (purple) associated with IB4$^+$ blood vessels (green), NG2$^+$ pericyte (red) coverage of IB4$^+$ vessels (green) and protein (fibrinogen, red), and Ter119$^+$ RBC (red) leakage in retinas from the sham and 6 h, 1 day, and 3 days after retinal I/R groups. Scale bar, 50 μm. (B, D, F, and H) Quantifications of (A), (C), (E), and (G) ($n$ = 7 mice per group). (I) Representative confocal fluorescence images of TUNEL staining in the retinal center (Central), mid-periphery (Mid-Ph), and far periphery (Far-Ph) from the sham and 6 h, 1 day, and 3 days after retinal I/R groups. Scale bar, 20 μm. (J) Quantification of TUNEL-positive rates in retinas from the sham and 6 h, 1 day, and 3 days after retinal I/R groups ($n$ = 4 mice per group). The data are expressed as the mean ± standard error of the mean (SEM). All statistical significance was calculated using two-way analysis of variance (ANOVA). *$p$ < 0.05, **$p$ < 0.01, ***$p$ < 0.001, and ****$p$ < 0.0001; ns, not significant.

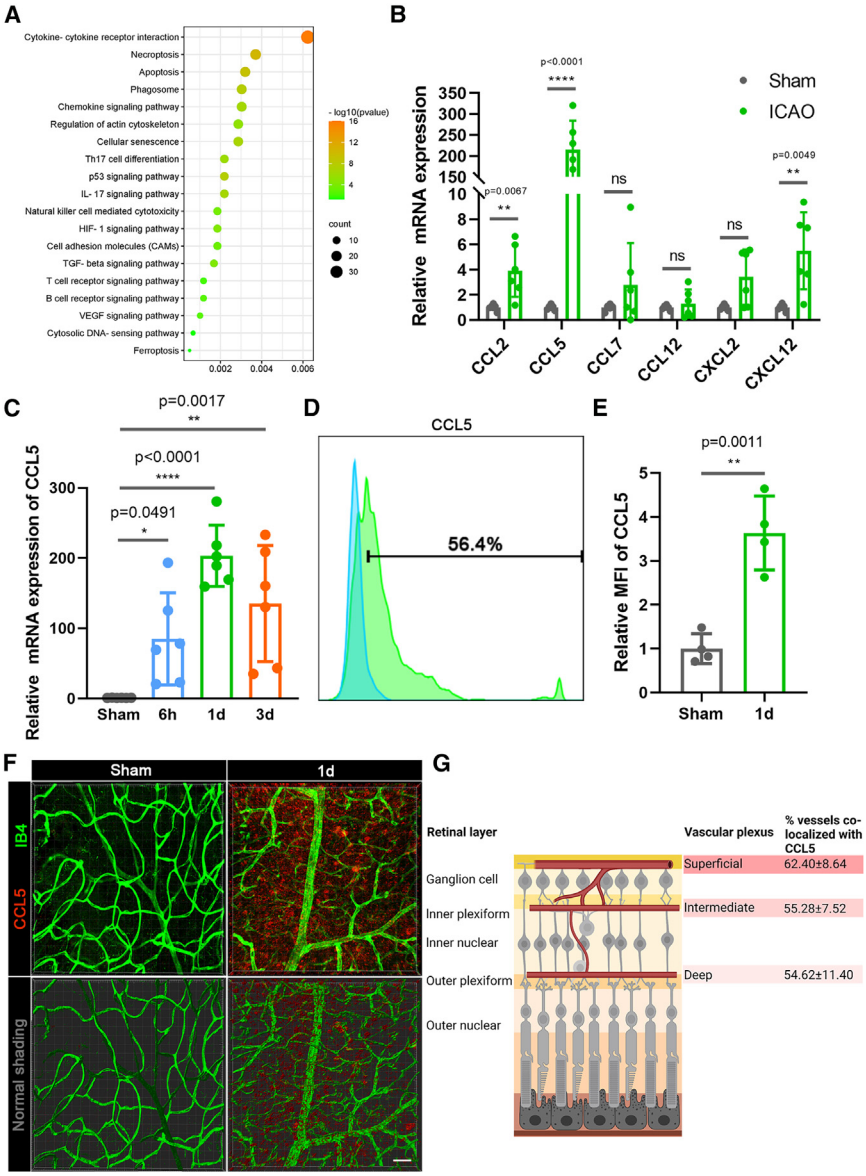


**Figure 2. CCL5 expression increased and colocalized with the BRB after retinal I/R**

(A) KEGG pathway enrichment analysis was performed for retinas from the sham and 1 day after retinal I/R groups to explore the possible signaling pathways that changed after retinal I/R ($n$ = 3 mice per group). (B) RT-qPCR was performed to measure the expression of CCL2, CCL5, CCL7, CCL12, CXCL2, and CXCL12 in retinas from the sham and 1 day after retinal I/R groups ($n$ = 6 mice per group). (C) RT-qPCR was performed to compare the expression of CCL5 in retinas from the sham and 6 h, 1 day, and 3 days after retinal I/R groups ($n$ = 6 mice per group). (D and E) Flow cytometry analysis and quantification of the mean fluorescence intensity (MFI) of CCL5 in retinas from the sham and 1 day after retinal I/R groups ($n$ = 4 mice per group). (F) Representative confocal fluorescence images of the distribution of CCL5 (red) around IB4$^+$ blood vessels (green) in retinas from the sham and 1 day after retinal I/R groups. Scale bar, 50 μm. (G) Scheme (left) of the structure of the retina and the division of the retinal plexus into three layers, namely, the superficial, intermediate, and deep layers. Quantification (right) of the percentage of vessels colocalized with CCL5 in each layer. Analysis and statistics of colocalization were performed via ImageJ and a plug-in named coloc2. The data are expressed as the mean ± SEM. All statistical significance was calculated using Student's t test or two-way ANOVA. $^*p < 0.05$, $^{**}p < 0.01$, and $^{****}p < 0.0001$; ns, not significant.

iMSC$^{tdTomato}$ under the recruitment of human CCL5 (hCCL5) and murine CCL5 (mCCL5), respectively. *In vitro*, transwell migration assays revealed that iMSC$^{CCR5}$ had greater migratory capacity than iMSC$^{tdTomato}$ in both the hCCL5 and mCCL5 groups, and human iMSC$^{CCR5}$ also responded to mCCL5 (Figures 3A and 3B). Next, we explored whether iMSC$^{CCR5}$ also had greater migratory and planting capacity *in vivo*. One day after retinal I/R, the mice from the I/R groups and sham groups both received intravitreal injections of iMSC$^{tdTomato}$ or iMSC$^{CCR5}$. Then, the mice were sacrificed at 4 days post-transplantation (4 dpt) and 7 dpt, and the number and biodistribution of iMSCs in the retina were detected and quantified. Compared with iMSC$^{tdTomato}$, iMSC$^{CCR5}$ preferentially migrated and integrated into the BRB at both 4 and 7 dpt in the I/R groups but not in the sham groups (Figures 3C and 3D). Overall, we successfully established a homogeneous iMSC lineage and overexpressed CCR5 in iMSCs. Additionally, we demonstrated that iMSC$^{CCR5}$ exhibited increased migratory capacity *in vitro* and was preferably integrated into the BRB as a biopatch *in vivo*.

### iMSC$^{CCR5}$ infusion protected against damage to the BRB and visual function caused by retinal I/R

Since iMSC$^{CCR5}$ migrated and integrated to blood vessels, we focused on whether iMSC$^{CCR5}$ could effectively restore BRB integrity as well as retinal function after retinal I/R. For this purpose, mice received intravitreal injections of phosphate buffer saline (PBS), iMSC$^{tdTomato}$, or iMSC$^{CCR5}$ at 1 day after retinal I/R, and retinas were obtained at 7 days after iMSC injection for further investigation (Figure 4A). First, we employed immunofluorescence staining to detect the integrity of the BRB. Compared with the PBS and iMSC$^{tdTomato}$ groups, the iMSC$^{CCR5}$ group presented less attenuation of Claudin5 coverage and pericyte coverage and less leakage of RBCs and fibrinogen, suggesting that iMSC$^{CCR5}$ effectively restored BRB integrity (Figures 4B–4D, 4F, S6A, and S6B). In addition, TUNEL staining revealed decreased degrees of apoptosis in each position of the retina (Figure 4E). Furthermore, iMSC$^{CCR5}$ treatment effectively increased the amplitudes of a- and b-waves and decreased implicit times compared with those in the

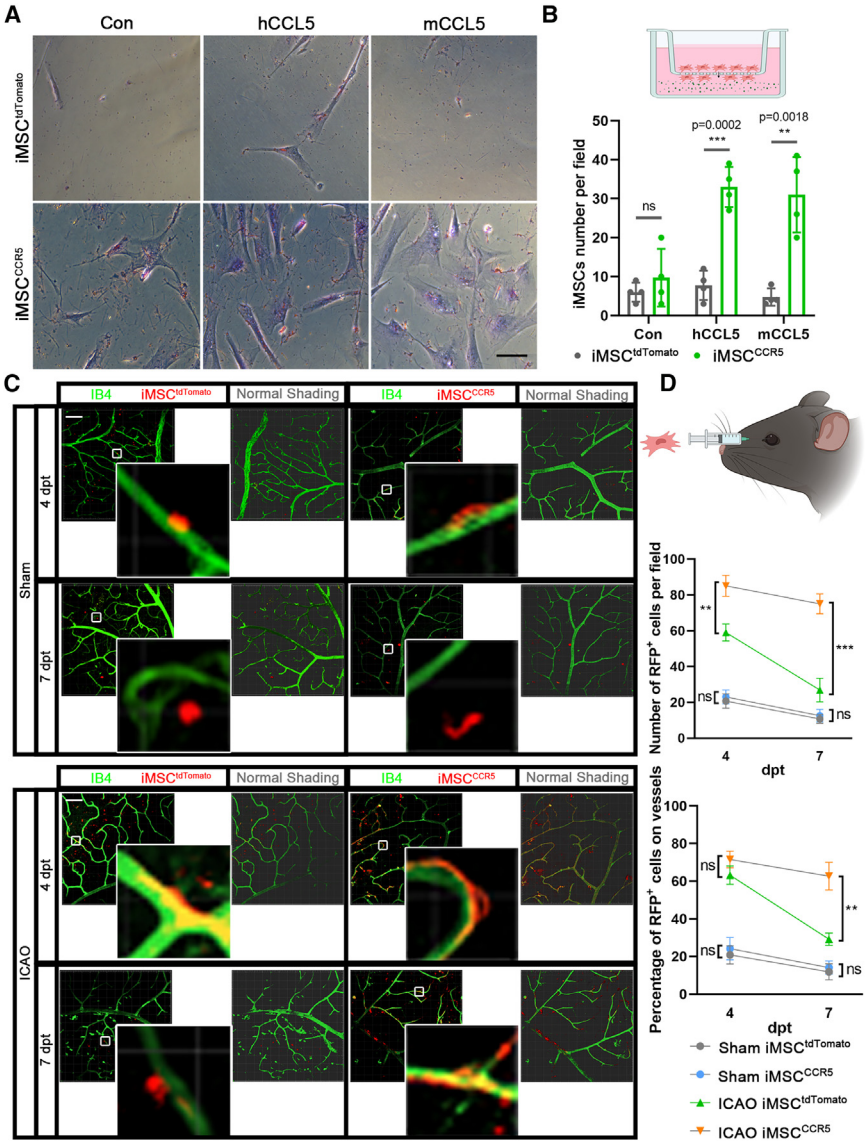


**Figure 3. Overexpression of CCR5 improved the migratory capacity of iMSCs *in vitro* and the vascular colonization capacity of iMSCs *in vivo***

(A) Transwell migration assays were performed to compare the migratory capacity of iMSC$^{tdTomato}$ and iMSC$^{CCR5}$ under the recruitment of hCCL5 and mCCL5, respectively. Scale bars, 100 μm. (B) Pattern (upward) and quantification of the transwell migration assay results. (C) Representative images of iMSC$^{CCR5}$ (red) and iMSC$^{tdTomato}$ (red) retained in retinas at 4 and 7 dpt from the sham and retinal I/R groups. Scale bar, 100 μm. (D) Pattern (top) and quantification analyses of the numbers of iMSC$^{CCR5}$ and iMSC$^{tdTomato}$ retained in retinas and their percentages on vessels at 4 and 7 dpt in the sham and retinal I/R groups ($n$ = 6 mice per group). The data are expressed as the mean ± SEM. All statistical significance was calculated using one-way or two-way ANOVA. $^{**}p < 0.01$ and $^{***}p < 0.001$; ns, not significant.

PBS and iMSC$^{tdTomato}$ treatments, suggesting retinal function recovery, as shown by electroretinography (ERG) (Figures 5A and 5B). Besides, we also focused on the long-term effect of iMSC$^{CCR5}$ treatment on retinal function recovery. ERG was analyzed 2 months after iMSC$^{CCR5}$ injection, and the results showed that iMSC$^{CCR5}$ treatment enhanced retinal function recovery compared with PBS and iMSC$^{tdTomato}$ treatments in the long term (Figures S7A and S7B). Taken together, these findings suggested that intravitreal injection of iMSC$^{CCR5}$ could protect against BRB damage and enhance retinal function recovery following retinal I/R.

In conclusion, we revealed BRB breakdown following retinal I/R and the resulting vascular content leakage, eventually leading to retinal cell death. Next, we found that the chemokine-chemokine receptor pathway was significantly involved in retinal I/R-related changes and that CCL5 expression increased most markedly and strongly colocalized with the BRB. Then, we generated the iMSC$^{CCR5}$ lineage, which exhibited better migratory capacity *in vitro*. *In vivo*, iMSC$^{CCR5}$, acting as biopatches, could enhance BRB integrity via direct integration into the BRB, thus improving retinal function recovery after retinal I/R (Graphical Abstract).

## DISCUSSION

In the present study, retinal I/R led to BRB breakdown and vascular content leakage, resulting in retinal cell death and the deterioration of visual function. Additionally, we examined the changes in the spectrum of chemokines following retinal I/R and found that CCL5 expression increased most markedly and remarkably around retinal vessels. Given the importance of the chemokine/chemokine receptor axis in cell migration, we engineered iMSC$^{CCR5}$, which displayed enhanced migratory capacity *in vitro*. *In vivo*, infused iMSC$^{CCR5}$ preferentially migrated and directly integrated into the BRB, which notably patched the BRB and improved the retinal function recovery after retinal I/R.

Given their tissue regeneration capacity and safety, MSCs have become potential candidates for cell therapy and translational medicine. The application of MSC-based therapy is promising for treating I/R in both peripheral organs and the central nervous system (CNS) through multiple mechanisms.[35] In peripheral organs, exogenous MSCs mainly protect parenchymal cells directly against I/R injury through their anti-apoptotic, anti-inflammatory, or antioxidative effects. For example, MSC-derived microRNA had cardioprotective effects against myocardial I/R injury by improving inflammation and

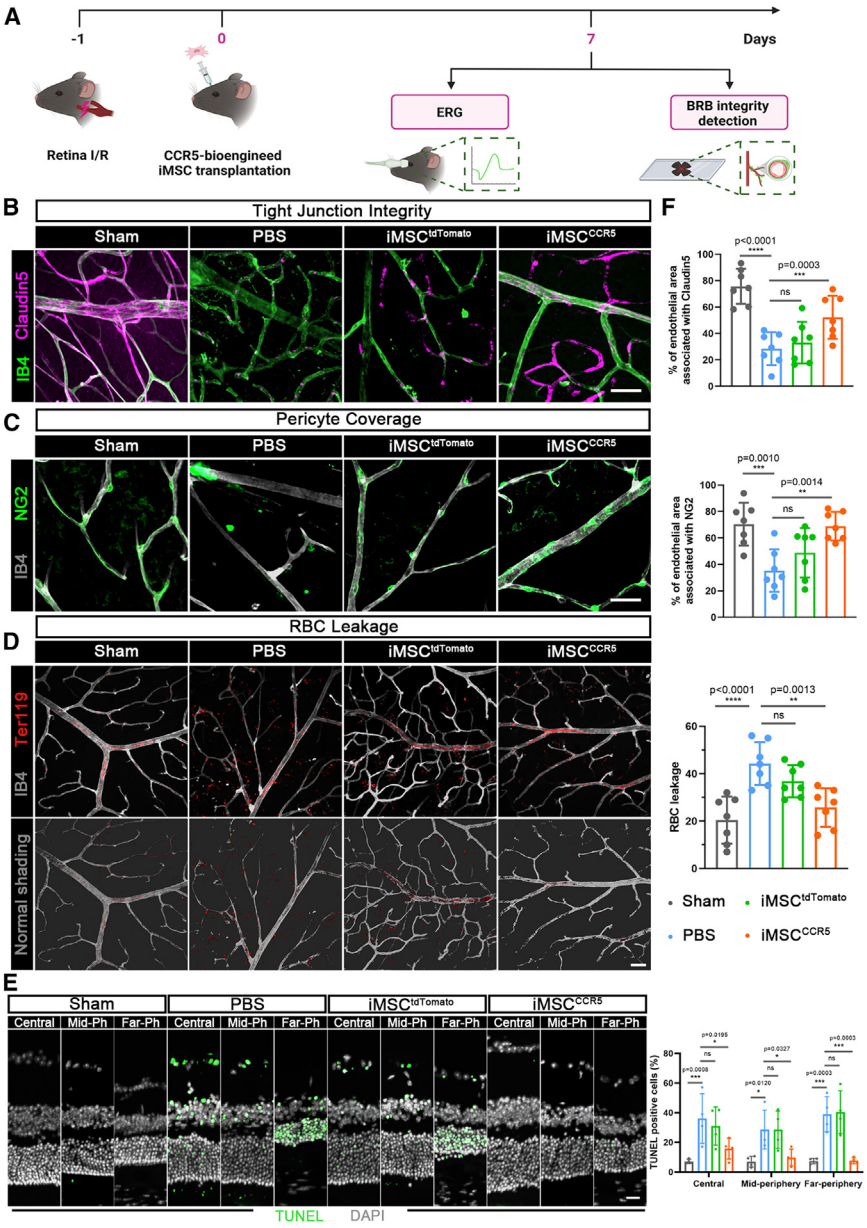


**Figure 4. iMSC$^{CCR5}$ infusion reversed damage to the BRB caused by retinal I/R**

(A) Scheme of the evaluation of iMSC-based therapy on retinal I/R. (B–D and F) Representative confocal fluorescence images and quantification of the distribution of Claudin5 (purple) associated with IB4$^{+}$ blood vessels (green), NG2$^{+}$ pericyte (green) coverage of IB4$^{+}$ blood vessels (gray), and Ter119$^{+}$ RBC (red) leakage in retinas from the sham, PBS, iMSC$^{tdTomato}$, and iMSC$^{CCR5}$ groups ($n$ = 7 mice per group). Scale bar, 50 μm. (E) Representative confocal fluorescence images of TUNEL staining and quantification of TUNEL-positive rates in the Central, Mid-Ph, and Far-Ph positions of retinas from the sham, PBS, iMSC$^{tdTomato}$, and iMSC$^{CCR5}$ groups ($n$ = 4 mice per group). Scale bar, 20 μm. The data are expressed as the mean ± SEM. All statistical significance was calculated using one-way or two-way ANOVA. $^{*}p < 0.05$, $^{**}p < 0.01$, $^{***}p < 0.001$, and $^{****}p < 0.0001$; ns, not significant.

pyroptosis in myocardial cells.[36] Additionally, MSCs had an anti-apoptotic effect on alveolar epithelial cells and ameliorated I/R injury after lung transplantation.[37] Furthermore, in renal I/R, MSC-EVs protected tubular epithelial cells against oxidative insult.[38] On the other hand, unlike peripheral organs, CNS homeostasis maintenance requires specialized vascular barrier integrity, which is indispensable for immune privilege and a defined microenvironment of the CNS. Given the importance of the CNS barrier, it is believed that MSCs not only protect against neuronal apoptosis but also restore the integrity of the BBB to avoid downstream damage after ischemic stroke.[39] Similarly, in our study, we also reported that iMSCs restored the integrity of the BRB and alleviated the apoptosis of retinal neural cells after retinal I/R. Based on the special structure and function of these barriers discussed above and our findings, protection and repair of these barriers constitute unique therapeutic mechanisms of MSC-based therapy for I/R injury to the CNS.

The BBB and BRB, as blood-neural barriers, have similar structures and play an important role in reliable neuronal activity by maintaining a precisely adjustable microenvironment.[40] The BBB is the bridge between blood and brain tissue and is composed mainly of brain capillary endothelial cells, base membrane, glial membrane, and peripheral pericytes and astrocytes. These specifically and finely developed structures allow the BBB to mechanically prevent substances such as toxins, drugs, and pathogens from entering the brain. In addition, due to the existence of different types of transporters on endothelial cells, nutrients and metabolites can smoothly pass through to maintain the homeostasis of the microenvironment of the nervous system. The intact BBB structure and functions are essential for structural and functional brain connectivity, synaptic activity, and information processing.[41] Similarly, the BRB is a typical neurovascular unit that is characteristic of the retina.[42] Suggested to be composed of tightly conjunct endothelial cells combined with pericytes, astrocytes, microcytes, and Müller cells, the BRB shares an analogous mechanism with the BBB in that it excludes immune cells and prevents disturbing substances from entering retinal tissue.[43] Breakdown of the BBB or BRB, induced by pathologically increased levels of VEGF or other mediators in the occurrence of pathological conditions such as trauma, I/R, or tumor, can result in vasogenic

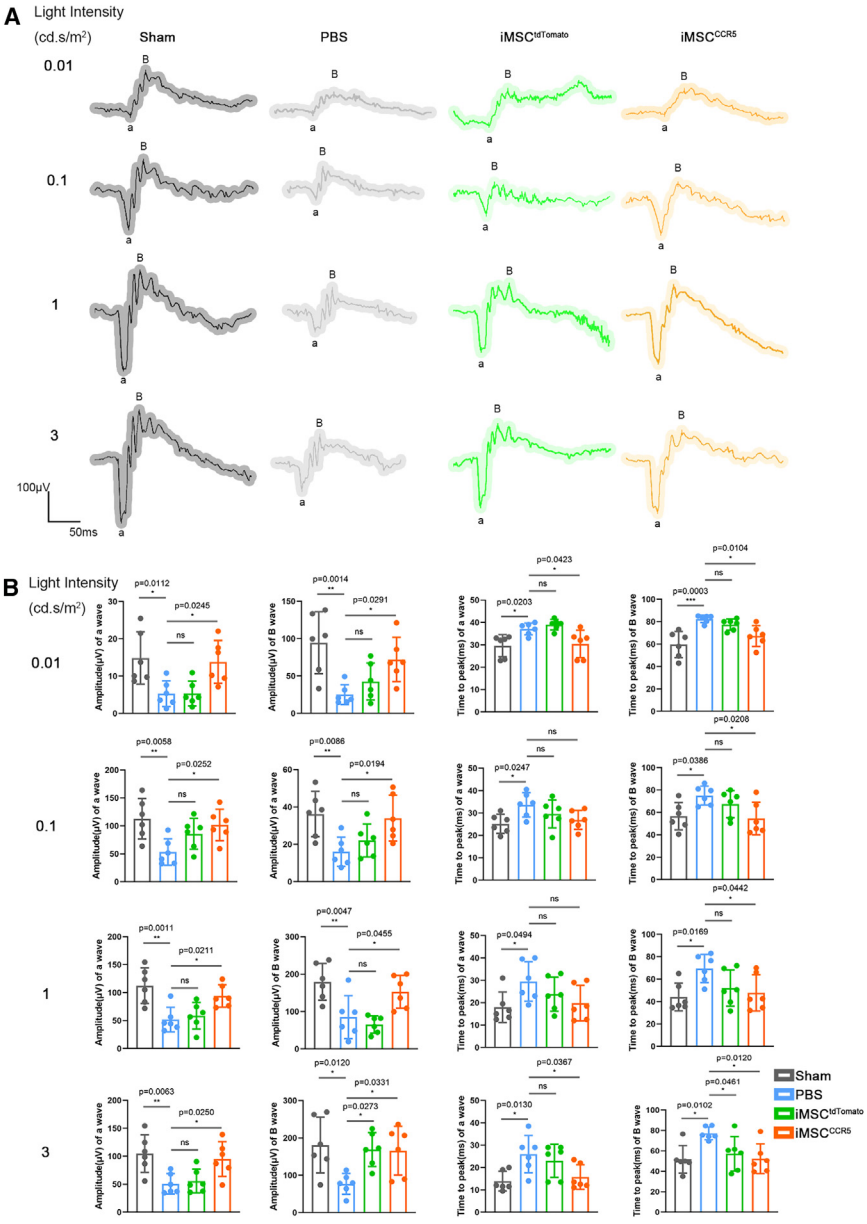


**Figure 5. iMSC$^{CCR5}$ infusion recovered damage to visual function caused by retinal I/R**

(A and B) ERG of amplitude and the time to peak of a- and b-waves among the sham, PBS, iMSC$^{tdTomato}$, and iMSC$^{CCR5}$ groups ($n$ = 6 mice per group). The light intensity consisted of 4 increasing levels (dim to bright), including 0.01, 0.1, 1, and 3 cd s/m$^2$. The data are expressed as the mean ± SEM. All statistical significance was calculated using one-way ANOVA. *$p$ < 0.05, **$p$ < 0.01, and ***$p$ < 0.001; ns, not significant.

edema and significant clinical problems such as brain morbidity or vision loss, respectively.[44]

MSC-based therapy for CNS barrier preservation is promising. For BBB preservation, MSCs are mainly given by intravenous injection. As most intravenously infused MSCs are distributed in the lungs, pulmonary microembolism is considered as an adverse effect.[45] Although MSCs are capable of transendothelial migration to infiltrate the brain, reaching enough cells for treatment is difficult.[46] Therefore, for safety and efficacy considerations, the intravenous injection of MSC-EVs is superior to the intravenous injection of MSCs for BBB treatment because of their small diameter and ability to cross the BBB. MSC-EVs stabilize the integrity of the BBB by enhancing Notch1 signaling in endothelial cells, upregulating VEGF receptor 1 expression in pericytes,[47] or inhibiting nuclear transcription factor κB signaling in astrocytes.[48] The above limitations of MSCs could be avoided by intravitreal injection for BRB preservation. In addition to repairing barriers through biochemical mechanisms similar to those of MSC-EVs, the structural support capacity of MSCs is advantageous over that of MSC-EVs.[45] In our study, we found that iMSCs can directly integrate into the BRB and act as biopatches for BRB preservation. Our results showed that iMSCs are promising future therapeutic candidates for treating retinal I/R-related diseases.

## MATERIALS AND METHODS

### Ethics statement

All animal experiments in this study complied with the guidelines of Sun Yat-sen University and were approved by the Ethics Committee of Sun Yat-sen University (2021001559, 2024 000008).

### Animals and retinal I/R model

Male wild-type (WT) C57BL/6 mice (8–10 weeks old) were purchased from Guangdong Medical Laboratory Animal Center (Guangzhou, China). All mice were provided free access to a standard rodent diet and drinking water and were kept in a colony room with a 12 h light/12 h dark cycle at the Sun Yat-sen University Animal Center. The ICA provides blood to the retina through the ophthalmic artery[49]; thus, the retinal I/R model was generated as follows: the mice were anesthetized with 1.5% isoflurane in a 30% $O_2$/69% $N_2O$ mixture, and a heating pad was used to maintain the body temperature at 37°C ± 0.5°C. Unilateral ligation (left side) of the ICA was performed using a 6/0 surgical suture for 40 min of ischemia, after which the suture was removed to allow reperfusion for 6 h, 1 day, or 3 days.

### Generation and identification of iMSCs

To differentiate hiPSCs into MSCs, the procedure was performed as previously described.[16] First, hiPSCs established as described were differentiated into neuromesodermal progenitors (NMPs).[50] Confluent hiPSCs were isolated into single cells by incubation with Accutase for 2–3 min at 37°C. Single cells were subsequently seeded into Matrigel-coated plates and cultured for 24 h in mTeSR medium supplemented with 10 μM Y27632 (Sigma-Aldrich, St. Louis, MO, USA). For NMP differentiation, these cells were then cultured in Essential 6 Medium containing 20 ng/mL basic fibroblast growth factor (bFGF), with or without 2–5 ng/mL transforming growth factor β1 (TGF-β1) (both from Pepro Tech, Rocky Hill, NJ, USA), and 10 μM Chir99021 (Stemgent, Cambridge, MA, USA) for 2–5 days. For MSC differentiation, paraxial mesoderm cells that had been differentiated in medium supplemented with bFGF, TGF-β1, and Chir99021 for 4–5 days were subsequently cultured in MesenCult-ACF Plus Medium (STEMCELL Technologies, Vancouver, Canada) for 2–3 weeks. The typical markers of MSCs were identified through flow cytometry as described below.

### Cell culture

iMSCs were cultured in MesenCult-ACF Plus Medium supplemented with 10% fetal bovine serum (FBS) and 1% penicillin and streptomycin and incubated in 5% $CO_2$ at 37°C.

### Multiple differentiation potential of iMSCs

Multiple differentiation assays, including osteogenic induction, adipogenic induction, and chondrogenic induction, were performed as previously described.[51,52] For osteogenic induction, iMSCs were cultured in alpha MEM supplemented with 100 nM dexamethasone, 10 mM β-glycerophosphate, 50 mM ascorbic acid-2-phosphate (Sigma-Aldrich), 10% FBS, and 1% penicillin and streptomycin for 21 days. Then, the osteoblasts were fixed in cold 95% ethanol for 5 min and stained with 2% alizarin red solution.

For adipogenic induction, iMSCs were cultured in alpha MEM supplemented with 1 mM dexamethasone, 500 mM 3-isobutyl-1-methylxanthine, 10 mg/mL insulin, 100 mM indomethacin (Sigma-Aldrich), 10% FBS, and 1% penicillin and streptomycin for 21 days. Subsequently, the resulting cells were fixed with 4% paraformaldehyde (PFA; Phygene, Fuzhou, China) for 30 min at room temperature and stained with fresh oil red O solution for 50 min.

For chondrogenic induction, the cells were cultured in a 15 mL conical tube containing differentiation basal medium (Sigma-Aldrich), which was changed every 3 days. After 21 days, the cell clumps were fixed in 4% PFA and stained with toluidine blue.

### Intravitreal injection

Intravitreal injection was performed under a stereomicroscope as previously described.[53] The mice were anesthetized as described above, and then the eyes were prepped with topical anesthetic. A cell suspension containing $1 \times 10^4$ iMSCs in 0.5 μL of PBS was slowly injected into the vitreous cavity of model eyes via a microinjector (Hamilton, Shanghai, China). The same volume of PBS was injected into the eyes of the control group.

### Retina processing and immunofluorescence

The mice were anesthetized as described above and perfused with ice-cold saline followed by 4% PFA. For immunofluorescence of whole-mounted neural retinas, eyeballs were removed and fixed in 4% PFA for 15 min at 4°C. After the cornea and crystalline lens were removed, the residual part was fixed in 4% PFA for 3 h at 4°C. The retinas were removed by orbital dissection, washed with PBS, and permeabilized in PBS containing 5% bovine serum albumin (Phygene) and 0.5% Triton X-100 (Sangon Biotech, Shanghai, China) overnight at 4°C. For immunofluorescence of retinal sections, eyeballs were removed, fixed in 4% PFA overnight at 4°C, and cut into 20 μm frozen cryosections. Retinal sections were fixed in 4% PFA for 20 min, permeabilized in 0.15% Triton X-100 for 15 min, and blocked with PBS-5% normal goat serum (BOSTER, Pleasanton, CA, USA) for 1 h. Both whole-mounted neural retinas and retinal sections were incubated with appropriate primary and secondary antibodies. Images were captured using Dragonfly high-speed confocal microscopy (ANDOR, Oxford Instruments, Oxford, UK). For the immunofluorescence of cells, the hiPSCs were fixed with 4% PFA at room temperature for 20 min and rinsed three times with PBS. Then, the cells were permeabilized with 0.3% Triton X-100 in PBS and incubated overnight at 4°C with primary antibodies. Secondary antibodies were incubated for 2 h at room temperature. The samples were counterstained with 4′,6-diamidino-2-phenylindole (DAPI; Sigma-Aldrich). Images were captured using a confocal laser-scanning microscope (LSM 880; Carl Zeiss, Jena, Germany). All of the utilized antibodies are listed in Table S1.

### TUNEL staining

The number of apoptotic cells in neural retinas was determined via TUNEL staining using a TUNEL Apoptosis Assay Kit (Thermo Fisher Scientific, Waltham, MA, USA), and the nuclei were stained with DAPI. Images were captured using Dragonfly high-speed confocal microscopy.

### Isolation of retinal and cellular RNA and real-time quantative PCR (RT-qPCR)

The mice were directly sacrificed by an overdose of sodium pentobarbital without perfusion, after which the retinas were removed and dissociated. For iMSCs, cell pellets were collected. Total RNA was extracted from retinas or iMSCs using an RNeasy mini kit (QIAGEN, Duesseldorf, Germany) according to the manufacturer's instructions, and RNA quality control was performed using a Nanodrop 2000 (Thermo Fisher Scientific). Then, cDNA was reverse transcribed using a Revert-Aid First Strand cDNA Synthesis Kit (Thermo Fisher Scientific). SYBR Green qPCR SuperMix (Roche, Basel, Switzerland) was used to conduct RT-qPCR, which was performed using a Light Cycler 480 detection system (Roche) as previously described.[54] The sequences of primers used in this study are presented in Table S4.

### Flow cytometric analysis of retinas and iMSCs

The mice were anesthetized as described above and perfused with ice-cold saline followed by 4% PFA, and the retinas were isolated. The retinas were mechanically homogenized and passed through 40 μm filters. For iMSCs, the cells were trypsinized and collected. After centrifugation, the cell pellets were resuspended and washed 3 times with PBS. Both the retinal cell suspension and the iMSCs were stained with the appropriate antibodies listed in Table S2. Fluorescence-activated cell sorting (FACS) was performed using CytoFLEX and CytoFLEX S (Beckman Coulter, CA, USA) flow cytometers.

### Western blotting

The cells were extracted and sonicated in radio immunoprecipitation assay lysis buffer (Beyotime, Shanghai, China) containing protease and phosphatase inhibitors (Roche), and the resulting supernatant was centrifuged. The protein concentration was then measured using a BCA protein assay kit (Cwbiotech, Beijing, China) and normalized across samples. Equal amounts of protein were resolved and separated by sodium dodecyl sulfate-polyacrylamide gel electrophoresis and then electrotransferred onto a 0.45 μm pore size polyvinylidene difluoride membrane (Millipore, Boston, MA, USA). The membranes were blocked with 5% nonfat milk (Phygene) for 1 h and then incubated with the appropriate primary antibodies overnight at 4°C. Specifically, bound primary antibodies were detected using horseradish peroxidase-coupled secondary antibodies and enhanced chemiluminescence (Millipore). The primary and secondary antibodies are listed in Table S3.

### Vector construction and lentiviral transduction

To generate $iMSC^{tdTomato}$ and $iMSC^{CCR5}$ lines, lentiviruses containing the tdTomato vector and CCR5-overexpressing vector, respectively, were purchased from WZ Biosciences (Shandong, China). Before lentiviral transduction, iMSCs were seeded into 24-well plates and incubated in 5% $CO_2$ at 37°C overnight. The optimal cell density for lentiviral transduction is approximately 50%. The medium was subsequently removed, and 2 mL of fresh complete medium supplemented with 6 μg/mL polybrene was added. The lentiviruses were added to the cells at an MOI of 10. Twenty-four hours later, the medium containing the lentiviruses was replaced with fresh medium. At 48–72 h after lentiviral transduction, the expression of red fluorescence protein (RFP) was observed via fluorescence microscopy to determine the transfection efficiency. Then, the $RFP^+$ iMSCs were sorted through FACS and used for subsequent experiments. RT-qPCR and western blotting were performed to detect the CCR5 mRNA and protein levels, respectively, in the $iMSC^{CCR5}$ line.

### Transwell migration assay

Transwell migration assays were performed using transwell chambers (24-well plate, 8 μm pore size; Corning, Corning, NY, USA). $iMSC^{CCR5}$ or $iMSC^{tdTomato}$ was suspended in serum-free medium and adjusted to a density of $1 \times 10^5$ cells/mL. 100 μL of cell suspension was added to the upper chamber of the migration well. In contrast, 100 μL of serum-free medium supplemented with the chemokine mCCL5 (100 ng/mL) or hCCL5 (50 ng/mL) (MedChem Express, Monmouth Junction, NJ, USA) was loaded into the lower chamber. Twenty-four hours later, the cells that migrated through the underside of the insert membrane were fixed with 4% PFA for 30 min and stained with crystal violet (Beyotime) for 20 min. Then, the cells in five random separate microscope fields were counted (400× magnification).

### ERG

To evaluate the visual function of the mice, photopic flash ERG was performed using the Diagnosys Espion system (Diagnosys, Lowell, MA, USA). To demonstrate the effect of iMSC treatment, ERG was performed at 1 week after intravitreal injection. Before the ERG test, the mice were incubated in a dark environment for 12 h and then anesthetized as described above, after which the pupils were dilated with 0.5% tropicamide (Macklin, Shanghai, China). Ring-shaped gold recording electrodes were placed on the cornea of both eyes. A pair of reference needle electrodes made of stainless steel were placed subcutaneously behind the ears, and a ground electrode was placed subcutaneously by the tail. After 10 min of adaptation to green light at 5 cd s/$m^2$, the eyes of the tested mouse were exposed to a series of light flashes ranging from 0.01 to 3 cd s/$m^2$, with 32 flashes at each light intensity and a 0.5 s interval of each flash. The body temperature of the mice was maintained at 37°C ± 0.5°C with a heating pad throughout the entire procedure. The results were analyzed for a-wave, b-wave, and implicit time using ERGView 4.380R software (OcuScience, Henderson, NV, USA).

### KEGG pathway analysis

Transcriptome sequencing was performed by Suzhou PANOMIX Biomedical Tech. KEGG pathway enrichment analysis was performed via the Bioconductor package "GeneAnswers" to identify critical pathways closely related to the impact of I/R on the retina. $p < 0.05$ was considered to indicate statistical significance and achieve significant enrichment.

### GSEA

GSEA was conducted, and the plots were generated at http://www.webgestalt.org/. All $p$ values were corrected for multiple testing methods, and the thresholds for significant enrichment were $p < 0.05$ and false discovery rate (FDR) < 0.25.

### Scheme creation

All the schemes used in this study were created with BioRender (BioRender, Toronto, Canada; https://www.biorender.com/).

### Statistical analysis

GraphPad Prism 8 software (San Diego, CA, USA) was used for all the statistical analyses. ImageJ 1.52a software (Wayne Rasband, MD, USA) was used to analyze the immunostaining images. CytExpert 2.0 software (Beckman Coulter) and FlowJo v.10.0 software (Mario Roederer, OR, USA) were used to analyze the FACS data. Ingenuity Pathway Analysis (IPA; v.52912811) software (Ingenuity Systems) was used to analyze the RNA sequencing (RNA-seq) data. The data obtained from multiple experiments were presented as the

mean ± SEM. Depending on the data, a Student's t test and one-way and two-way analysis of variance (ANOVA) were used for comparisons and are indicated in the legends of each figure. Differences were considered significant when $p < 0.05$.

## DATA AND CODE AVAILABILITY

The data that support the findings of this study are available from the corresponding author upon reasonable request.

## ACKNOWLEDGMENTS

This study was supported by the National Natural Science Foundation of China (grant 82271093 and 82070972 to Tao Li), China Post-doctoral Science Foundation (grant 2023M744060 to Xiaoyue Wei), Guangdong Basic and Applied Basic Research Foundation (grant 2023A1515110138 to Xiaoyue Wei). We would like to thank other members from the State Key Laboratory of Ophthalmology, Sun Yat-Sen University, and the Center of Stem Cells and Tissue Engineering, Sun Yat-Sen University, for their help and suggestions. The graphical abstract was created using BioRender.

## AUTHOR CONTRIBUTIONS

X.W., H.M., and Q.Z. designed and performed the experiments. Z.Z. and Y.R. analyzed the data and wrote the manuscript. K.L., Y.M., and Z.L. performed the statistical analysis. R.T. and Z.C. conducted the investigation. A.P.X. and T.L. supervised the study. All the authors read and approved the final manuscript.

## DECLARATION OF INTERESTS

The authors declare that they have no competing interests.

## SUPPLEMENTAL INFORMATION

Supplemental information can be found online at https://doi.org/10.1016/j.omtn.2024.102445.

## REFERENCES

1. Lu, C., Wang, C., Xiao, H., Chen, M., Yang, Z., Liang, Z., Wang, H., Liu, Y., Yang, Y., and Wang, Q. (2021). Ethyl pyruvate: A newly discovered compound against ischemia-reperfusion injury in multiple organs. Pharmacol. Res. *171*, 105757. https://doi.org/10.1016/j.phrs.2021.105757.

2. Bresnick, G.H., De Venecia, G., Myers, F.L., Harris, J.A., and Davis, M.D. (1975). Retinal ischemia in diabetic retinopathy. Arch. Ophthalmol. *93*, 1300–1310. https://doi.org/10.1001/archopht.1975.01010020934002.

3. Tang, L.H.C., Fung, F.K.C., Lai, A.K.W., Wong, I.Y.H., Shih, K.C., and Lo, A.C.Y. (2021). Autophagic Upregulation Is Cytoprotective in Ischemia/Reperfusion-Injured Retina and Retinal Progenitor Cells. Int. J. Mol. Sci. *22*, 8446. https://doi.org/10.3390/ijms22168446.

4. Burton, M.J., Ramke, J., Marques, A.P., Bourne, R.R.A., Congdon, N., Jones, I., Ah Tong, B.A.M., Arunga, S., Bachani, D., Bascaran, C., et al. (2021). The Lancet Global Health Commission on Global Eye Health: vision beyond 2020. Lancet Global Health *9*, e489–e551. https://doi.org/10.1016/s2214-109x(20)30488-5.

5. Tan, G.S.W., Chakravarthy, U., and Wong, T.Y. (2020). Anti-VEGF Therapy or Vitrectomy Surgery for Vitreous Hemorrhage From Proliferative Diabetic Retinopathy. JAMA *324*, 2375–2377. https://doi.org/10.1001/jama.2020.22829.

6. Minhas, G., Sharma, J., and Khan, N. (2016). Cellular Stress Response and Immune Signaling in Retinal Ischemia-Reperfusion Injury. Front. Immunol. *7*, 444. https://doi.org/10.3389/fimmu.2016.00444.

7. Osborne, N.N., Casson, R.J., Wood, J.P.M., Chidlow, G., Graham, M., and Melena, J. (2004). Retinal ischemia: mechanisms of damage and potential therapeutic strategies. Prog. Retin. Eye Res. *23*, 91–147. https://doi.org/10.1016/j.preteyeres.2003.12.001.

8. Uccelli, A., Moretta, L., and Pistoia, V. (2008). Mesenchymal stem cells in health and disease. Nat. Rev. Immunol. *8*, 726–736. https://doi.org/10.1038/nri2395.

9. Oh, J.Y., and Lee, R.H. (2021). Mesenchymal stromal cells for the treatment of ocular autoimmune diseases. Prog. Retin. Eye Res. *85*, 100967. https://doi.org/10.1016/j.preteyeres.2021.100967.

10. Gu, C., Zhang, H., and Gao, Y. (2021). Adipose mesenchymal stem cells-secreted extracellular vesicles containing microRNA-192 delays diabetic retinopathy by targeting ITGA1. J. Cell. Physiol. *236*, 5036–5051. https://doi.org/10.1002/jcp.30213.

11. Mathew, B., Ravindran, S., Liu, X., Torres, L., Chennakesavalu, M., Huang, C.-C., Feng, L., Zelka, R., Lopez, J., Sharma, M., and Roth, S. (2019). Mesenchymal stem cell-derived extracellular vesicles and retinal ischemia-reperfusion. Biomaterials *197*, 146–160. https://doi.org/10.1016/j.biomaterials.2019.01.016.

12. Méndez-Ferrer, S., Michurina, T.V., Ferraro, F., Mazloom, A.R., Macarthur, B.D., Lira, S.A., Scadden, D.T., Ma'ayan, A., Enikolopov, G.N., and Frenette, P.S. (2010). Mesenchymal and haematopoietic stem cells form a unique bone marrow niche. Nature *466*, 829–834. https://doi.org/10.1038/nature09262.

13. Park, D., Spencer, J.A., Koh, B.I., Kobayashi, T., Fujisaki, J., Clemens, T.L., Lin, C.P., Kronenberg, H.M., and Scadden, D.T. (2012). Endogenous bone marrow MSCs are dynamic, fate-restricted participants in bone maintenance and regeneration. Cell Stem Cell *10*, 259–272. https://doi.org/10.1016/j.stem.2012.02.003.

14. Kim, S., Lee, S., Lim, J., Choi, H., Kang, H., Jeon, N.L., and Son, Y. (2021). Human bone marrow-derived mesenchymal stem cells play a role as a vascular pericyte in the reconstruction of human BBB on the angiogenesis microfluidic chip. Biomaterials *279*, 121210. https://doi.org/10.1016/j.biomaterials.2021.121210.

15. Costa, L.A., Eiro, N., Fraile, M., Gonzalez, L.O., Saá, J., Garcia-Portabella, P., Vega, B., Schneider, J., and Vizoso, F.J. (2021). Functional heterogeneity of mesenchymal stem cells from natural niches to culture conditions: implications for further clinical uses. Cell. Mol. Life Sci. *78*, 447–467. https://doi.org/10.1007/s00018-020-03600-0.

16. Wang, H., Li, D., Zhai, Z., Zhang, X., Huang, W., Chen, X., Huang, L., Liu, H., Sun, J., Zou, Z., et al. (2019). Characterization and Therapeutic Application of Mesenchymal Stem Cells with Neuromesodermal Origin from Human Pluripotent Stem Cells. Theranostics *9*, 1683–1697. https://doi.org/10.7150/thno.30487.

17. Ozay, E.I., Vijayaraghavan, J., Gonzalez-Perez, G., Shanthalingam, S., Sherman, H.L., Garrigan, D.T., Jr., Chandiran, K., Torres, J.A., Osborne, B.A., Tew, G.N., et al. (2019). Cymerus™ iPSC-MSCs significantly prolong survival in a pre-clinical, humanized mouse model of Graft-vs-host disease. Stem Cell Res. *35*, 101401. https://doi.org/10.1016/j.scr.2019.101401.

18. Wruck, W., Graffmann, N., Spitzhorn, L.-S., and Adjaye, J. (2021). Human Induced Pluripotent Stem Cell-Derived Mesenchymal Stem Cells Acquire Rejuvenation and Reduced Heterogeneity. Front. Cell Dev. Biol. *9*, 717772. https://doi.org/10.3389/fcell.2021.717772.

19. Zhou, T., Yuan, Z., Weng, J., Pei, D., Du, X., He, C., and Lai, P. (2021). Challenges and advances in clinical applications of mesenchymal stromal cells. J. Hematol. Oncol. *14*, 24. https://doi.org/10.1186/s13045-021-01037-x.

20. Kim, J.Y., Kim, S.H., Seok, J., Bae, S.H., Hwang, S.-G., and Kim, G.J. (2023). Increased PRL-1 in BM-derived MSCs triggers anaerobic metabolism via mitochondria in a cholestatic rat model. Mol. Ther. Nucleic Acids *31*, 512–524. https://doi.org/10.1016/j.omtn.2023.01.017.

21. Johnson, T.V., Bull, N.D., and Martin, K.R. (2009). Transplantation prospects for the inner retina. Eye *23*, 1980–1984. https://doi.org/10.1038/eye.2008.376.

22. Yu, S., Tanabe, T., Dezawa, M., Ishikawa, H., and Yoshimura, N. (2006). Effects of bone marrow stromal cell injection in an experimental glaucoma model. Biochem. Biophys. Res. Commun. *344*, 1071–1079.

23. Dhoke, N.R., Kaushik, K., and Das, A. (2020). Cxcr6-Based Mesenchymal Stem Cell Gene Therapy Potentiates Skin Regeneration in Murine Diabetic Wounds. Mol. Ther. *28*, 1314–1326. https://doi.org/10.1016/j.ymthe.2020.02.014.

24. Chen, W., Li, M., Cheng, H., Yan, Z., Cao, J., Pan, B., Sang, W., Wu, Q., Zeng, L., Li, Z., and Xu, K. (2013). Overexpression of the mesenchymal stem cell Cxcr4 gene in irradiated mice increases the homing capacity of these cells. Cell Biochem. Biophys. *67*, 1181–1191. https://doi.org/10.1007/s12013-013-9632-6.

25. Wynn, R.F., Hart, C.A., Corradi-Perini, C., O'Neill, L., Evans, C.A., Wraith, J.E., Fairbairn, L.J., and Bellantuono, I. (2004). A small proportion of mesenchymal stem cells strongly expresses functionally active CXCR4 receptor capable of promoting migration to bone marrow. Blood *104*, 2643–2645.

26. Vallet, S., Pozzi, S., Patel, K., Vaghela, N., Fulciniti, M.T., Veiby, P., Hideshima, T., Santo, L., Cirstea, D., Scadden, D.T., et al. (2011). A novel role for CCL3 (MIP-1α) in myeloma-induced bone disease via osteocalcin downregulation and inhibition of osteoblast function. Leukemia *25*, 1174–1181. https://doi.org/10.1038/leu.2011.43.

27. Muthusamy, A., Lin, C.M., Shanmugam, S., Lindner, H.M., Abcouwer, S.F., and Antonetti, D.A. (2014). Ischemia-reperfusion injury induces occludin phosphorylation/ubiquitination and retinal vascular permeability in a VEGFR-2-dependent manner. J. Cerebr. Blood Flow Metabol. *34*, 522–531. https://doi.org/10.1038/jcbfm.2013.230.

28. Liu, L., Jiang, Y., and Steinle, J.J. (2016). Compound 49b Restores Retinal Thickness and Reduces Degenerate Capillaries in the Rat Retina following Ischemia/Reperfusion. PLoS One *11*, e0159532. https://doi.org/10.1371/journal.pone.0159532.

29. DeDreu, J., Pal-Ghosh, S., Mattapallil, M.J., Caspi, R.R., Stepp, M.A., and Menko, A.S. (2022). Uveitis-mediated immune cell invasion through the extracellular matrix of the lens capsule. Faseb. J. *36*, e21995. https://doi.org/10.1096/fj.202101098R.

30. Wu, M.Y., Yiang, G.T., Liao, W.T., Tsai, A.P.Y., Cheng, Y.L., Cheng, P.W., Li, C.Y., and Li, C.J. (2018). Current Mechanistic Concepts in Ischemia and Reperfusion Injury. Cell. Physiol. Biochem. *46*, 1650–1667. https://doi.org/10.1159/000489241.

31. Kalogeris, T., Baines, C.P., Krenz, M., and Korthuis, R.J. (2012). Cell biology of ischemia/reperfusion injury. Int. Rev. Cell Mol. Biol. *298*, 229–317. https://doi.org/10.1016/b978-0-12-394309-5.00006-7.

32. Zhang, Y., Zhao, L., Wang, X., Ma, W., Lazere, A., Qian, H.H., Zhang, J., Abu-Asab, M., Fariss, R.N., Roger, J.E., and Wong, W.T. (2018). Repopulating retinal microglia restore endogenous organization and function under CX3CL1-CX3CR1 regulation. Sci. Adv. *4*, eaap8492. https://doi.org/10.1126/sciadv.aap8492.

33. Kinuthia, U.M., Wolf, A., and Langmann, T. (2020). Microglia and Inflammatory Responses in Diabetic Retinopathy. Front. Immunol. *11*, 564077. https://doi.org/10.3389/fimmu.2020.564077.

34. Pesaresi, M., Bonilla-Pons, S.A., Sebastian-Perez, R., Di Vicino, U., Alcoverro-Bertran, M., Michael, R., and Cosma, M.P. (2021). The Chemokine Receptors Ccr5 and Cxcr6 Enhance Migration of Mesenchymal Stem Cells into the Degenerating Retina. Mol. Ther. *29*, 804–821. https://doi.org/10.1016/j.ymthe.2020.10.026.

35. Xie, L., Chen, Z., Liu, M., Huang, W., Zou, F., Ma, X., Tao, J., Guo, J., Xia, X., Lyu, F., et al. (2020). MSC-Derived Exosomes Protect Vertebral Endplate Chondrocytes against Apoptosis and Calcification via the miR-31-5p/ATF6 Axis. Mol. Ther. Nucleic Acids *22*, 601–614. https://doi.org/10.1016/j.omtn.2020.09.026.

36. Yue, R., Lu, S., Luo, Y., Zeng, J., Liang, H., Qin, D., Wang, X., Wang, T., Pu, J., and Hu, H. (2022). Mesenchymal stem cell-derived exosomal microRNA-182-5p alleviates myocardial ischemia/reperfusion injury by targeting GSDMD in mice. Cell Death Dis. *8*, 202. https://doi.org/10.1038/s41420-022-00909-6.

37. Nakajima, D., Watanabe, Y., Ohsumi, A., Pipkin, M., Chen, M., Mordant, P., Kanou, T., Saito, T., Lam, R., Coutinho, R., et al. (2019). Mesenchymal stromal cell therapy during ex vivo lung perfusion ameliorates ischemia-reperfusion injury in lung transplantation. J. Heart Lung Transplant. *38*, 1214–1223. https://doi.org/10.1016/j.healun.2019.07.006.

38. Cao, H., Cheng, Y., Gao, H., Zhuang, J., Zhang, W., Bian, Q., Wang, F., Du, Y., Li, Z., Kong, D., et al. (2020). In Vivo Tracking of Mesenchymal Stem Cell-Derived Extracellular Vesicles Improving Mitochondrial Function in Renal Ischemia-Reperfusion Injury. ACS Nano *14*, 4014–4026. https://doi.org/10.1021/acsnano.9b08207.

39. Qiu, L., Cai, Y., Geng, Y., Yao, X., Wang, L., Cao, H., Zhang, X., Wu, Q., Kong, D., Ding, D., et al. (2022). Mesenchymal stem cell-derived extracellular vesicles attenuate tPA-induced blood-brain barrier disruption in murine ischemic stroke models. Acta Biomater. *154*, 424–442. https://doi.org/10.1016/j.actbio.2022.10.022.

40. Kim, J.H., Kim, J.H., Park, J.A., Lee, S.-W., Kim, W.J., Yu, Y.S., and Kim, K.-W. (2006). Blood-neural barrier: intercellular communication at glio-vascular interface. J. Biochem. Mol. Biol. *39*, 339–345.

41. Zhao, Z., Nelson, A.R., Betsholtz, C., and Zlokovic, B.V. (2015). Establishment and Dysfunction of the Blood-Brain Barrier. Cell *163*, 1064–1078. https://doi.org/10.1016/j.cell.2015.10.067.

42. Mölzer, C., Heissigerova, J., Wilson, H.M., Kuffova, L., and Forrester, J.V. (2020). Immune Privilege: The Microbiome and Uveitis. Front. Immunol. *11*, 608377. https://doi.org/10.3389/fimmu.2020.608377.

43. Spadoni, I., Fornasa, G., and Rescigno, M. (2017). Organ-specific protection mediated by cooperation between vascular and epithelial barriers. Nat. Rev. Immunol. *17*, 761–773. https://doi.org/10.1038/nri.2017.100.

44. Bosma, E.K., van Noorden, C.J.F., Schlingemann, R.O., and Klaassen, I. (2018). The role of plasmalemma vesicle-associated protein in pathological breakdown of blood-brain and blood-retinal barriers: potential novel therapeutic target for cerebral edema and diabetic macular edema. Fluids Barriers CNS *15*, 24. https://doi.org/10.1186/s12987-018-0109-2.

45. Galipeau, J., and Sensébé, L. (2018). Mesenchymal Stromal Cells: Clinical Challenges and Therapeutic Opportunities. Cell Stem Cell *22*, 824–833. https://doi.org/10.1016/j.stem.2018.05.004.

46. Lou, Y.-L., Guo, F., Liu, F., Gao, F.-L., Zhang, P.-Q., Niu, X., Guo, S.-C., Yin, J.-H., Wang, Y., and Deng, Z.-F. (2012). miR-210 activates notch signaling pathway in angiogenesis induced by cerebral ischemia. Mol. Cell. Biochem. *370*, 45–51. https://doi.org/10.1007/s11010-012-1396-6.

47. Jean LeBlanc, N., Guruswamy, R., and ElAli, A. (2018). Vascular Endothelial Growth Factor Isoform-B Stimulates Neurovascular Repair After Ischemic Stroke by Promoting the Function of Pericytes via Vascular Endothelial Growth Factor Receptor-1. Mol. Neurobiol. *55*, 3611–3626. https://doi.org/10.1007/s12035-017-0478-6.

48. Park, H.J., Shin, J.Y., Kim, H.N., Oh, S.H., Song, S.K., and Lee, P.H. (2015). Mesenchymal stem cells stabilize the blood-brain barrier through regulation of astrocytes. Stem Cell Res. Ther. *6*, 187. https://doi.org/10.1186/s13287-015-0180-4.

49. Tamaki, M., Kidoguchi, K., Mizobe, T., Koyama, J., Kondoh, T., Sakurai, T., Kohmura, E., Yokono, K., and Umetani, K. (2006). Carotid artery occlusion and collateral circulation in C57Black/6J mice detected by synchrotron radiation microangiography. Kobe J. Med. Sci. *52*, 111–118.

50. Li, W., Huang, L., Zeng, J., Lin, W., Li, K., Sun, J., Huang, W., Chen, J., Wang, G., Ke, Q., et al. (2018). Characterization and transplantation of enteric neural crest cells from human induced pluripotent stem cells. Mol. Psychiatr. *23*, 499–508. https://doi.org/10.1038/mp.2016.191.

51. Li, L., Du, G., Wang, D., Zhou, J., Jiang, G., and Jiang, H. (2017). Overexpression of Heme Oxygenase-1 in Mesenchymal Stem Cells Augments Their Protection on Retinal Cells In Vitro and Attenuates Retinal Ischemia/Reperfusion Injury In Vivo against Oxidative Stress. Stem Cell. Int. *2017*, 4985323. https://doi.org/10.1155/2017/4985323.

52. Morikawa, S., Mabuchi, Y., Kubota, Y., Nagai, Y., Niibe, K., Hiratsu, E., Suzuki, S., Miyauchi-Hara, C., Nagoshi, N., Sunabori, T., et al. (2009). Prospective identification, isolation, and systemic transplantation of multipotent mesenchymal stem cells in murine bone marrow. J. Exp. Med. *206*, 2483–2496. https://doi.org/10.1084/jem.20091046.

53. Jiang, D., Xiong, G., Feng, H., Zhang, Z., Chen, P., Yan, B., Chen, L., Gandhervin, K., Ma, C., Li, C., et al. (2019). Donation of mitochondria by iPSC-derived mesenchymal stem cells protects retinal ganglion cells against mitochondrial complex I defect-induced degeneration. Theranostics *9*, 2395–2410. https://doi.org/10.7150/thno.29422.

54. Liu, J., Li, W., Wang, Y., Fan, W., Li, P., Lin, W., Yang, D., Fang, R., Feng, M., Hu, C., et al. (2014). Islet-1 overexpression in human mesenchymal stem cells promotes vascularization through monocyte chemoattractant protein-3. Stem Cell. *32*, 1843–1854. https://doi.org/10.1002/stem.1682.